HHS Public Access

Author manuscript

J Struct Biol. Author manuscript; available in PMC 2020 October 01.

Published in final edited form as:

J Struct Biol. 2019 October 01; 208(1): 18–29. doi:10.1016/j.jsb.2019.07.005.

Solution structural model of the complex of the binding regions of human plasminogen with its M-protein receptor from *Streptococcus pyogenes*

Yue Yuan[1], **Yetunde A. Ayinuola**[1], **Damini Singh**[1], **Olawole Ayinuola**[1], **Jeffrey A. Mayfield**[1], **Adam Quek**[2], **James C. Whisstock**[2], **Ruby H.P. Law**[2], **Shaun W. Lee**[3], **Victoria A. Ploplis**[1,4], **Francis J. Castellino**[1,4,*]

[1]W.M. Keck Center for Transgene Research, University of Notre Dame, Notre Dame, IN, USA 46556.

[2]Department of Biochemistry and Molecular Biology, Monash University, Clayton, 3800 VIC, Au.

[3]Department of Biological Sciences; University of Notre Dame, Notre Dame, IN, USA 46556.

[4]Department of Chemistry and Biochemistry; University of Notre Dame, Notre Dame, IN, USA. 46556

Abstract

VEK50 is a truncated peptide from a *Streptococcal pyogenes* surface human plasminogen (hPg) binding M-protein (PAM). VEK50 contains the full A-domain of PAM, which is responsible for its low nanomolar binding to hPg. The interaction of VEK50 with kringle 2, the PAM-binding domain in hPg ($K2_{hPg}$), has been studied by high-resolution NMR spectroscopy. The data show that each VEK50 monomer in solution contains two tight binding sites for $K2_{hPg}$, one each in the *a1*- (RH1; $R^{17}H^{18}$) and *a2*- (RH2; $R^{30}H^{31}$) repeats within the A-domain of VEK50. Two mutant forms of VEK50, *viz*., VEK50[RH1/AA] ($VEK50^{\Delta RH1}$) and VEK50[RH2/AA] ($VEK50^{\Delta RH2}$), were designed by replacing each RH with AA, thus eliminating one of the $K2_{hPg}$ binding sites within VEK50, and allowing separate study of each binding site. Using ^{13}C- and ^{15}N-labeled peptides, NMR-derived solution structures of VEK50 in its complex with $K2_{hPg}$ were solved. We conclude that the A-domain of PAM can accommodate two molecules of $K2_{hPg}$ docked within a short distance of each other, and the strength of the binding is slightly different for each site. The solution structure of the VEK50/$K2_{hPg}$, complex, which is a reductionist model of the PAM/hPg

*Corresponding author: Francis J. Castellino, W.M. Keck Center for Transgene Research, University of Notre Dame, Notre Dame, IN 46556, USA Telephone-574.631.8996; Telefax-574.631.8017; fcastell@nd.edu.

8.Author contributions

YY, YAA, DS, JAM, OA, performed the experiments and edited drafts of the manuscript; FJC, SWL, and VAP edited drafts of the manuscript and interpreted the results; AQ, RHPL, and JCW collaborated on the final draft; FJC organized the project, consulted on experiments, and prepared the final version of the manuscript.

7.Conflicts of interest

The authors declare that they do not have conflicts of interest.

complex, provides insights for the binding mechanism of PAM to a host protein, a process that is critical to *S. pyogenes* virulence.

Graphical Abstract

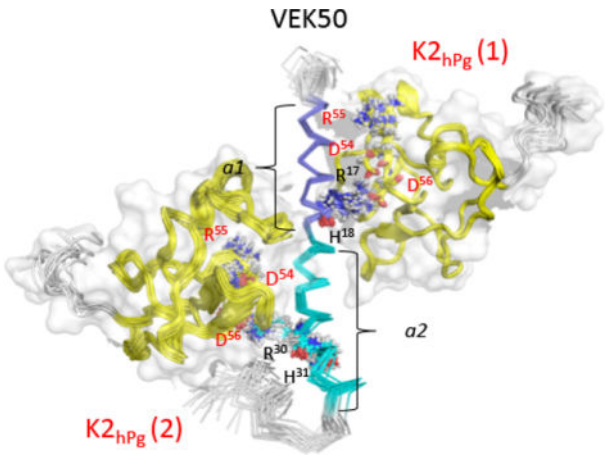

Keywords

Plasminogen binding; 3-D solution structure; bacterial receptor; modular proteins; a-repeats; peptide mutagenesis; NMR structures

1. Introduction

Approximately 250 serotypically distinct strains of Group A Streptococcus pyogenes (GAS) have been identified that present patients with mild to severe symptoms. The different GAS strains are serotyped through the nature of their characteristic surface M- and M-like proteins, with one skin-trophic subgroup (Pattern D) containing a direct human host plasminogen (hPg)/plasmin (hPm) surface M-protein receptor (PAM) (Berge and Sjobring, 1993). Binding of hPg to PAM-type M-proteins greatly facilitates its activation to the protease, hPm, by GAS- secreted streptokinase (SK), a step that is essential for its virulence (Sun et al., 2004). After activation, hPm remains bound to GAS, resulting in exacerbation of GAS pathogenicity through proteolytic disruption of host innate immune barriers to dissemination (Sanderson-Smith et al., 2008), *e.g.*, the extracellular matrix and tight cellular junctions (Lahteenmaki et al., 2000; Sumitomo et al., 2013; Sumitomo et al., 2016). The N-terminal A-domain of various PAM-type M-proteins usually consist of one or two peptide modules, viz., *a1*- and *a2*- repeats, having 13–17 residues each (Qiu et al., 2018). Both repeats have been shown to be critical determinants for hPg binding. (Ringdahl et al., 1998; Rios-Steiner et al., 2001; Sanderson-Smith et al., 2007; Schenone et al., 2000; Wang et al., 2010b; Yuan et al., 2017).

Contained within the hPg protein, the lysine binding site (LBS) of its small functionally-independent kringle 2 ($K2_{hPg}$) domain has been identified as the major receptor site for PAM binding (Wistedt et al., 1998). The LBS of four of the five kringle domains of hPg generally interact with activation effectors (Castellino and Ploplis, 2003), as well as with cellular

receptors (Pancholi and Fischetti, 1998), *via* C-terminal lysine residues of the receptor (Miles et al., 1991). However, the prototypical Pattern D GAS receptor for hPg, *e.g.*, PAM from isolate AP53 (PAM_{AP53}), does not contain a C-terminal lysine residue and interacts with hPg *via* an internal pseudo-lysine arrangement of amino acid side-chains (Rios-Steiner et al., 2001; Wang et al., 2010b; Yuan et al., 2017). In this regard, adjacent Arg and His residues in both the *a1*- and *a2*-repeats of the PAM A-domain have been shown to be essential for hPg binding (Rios-Steiner et al., 2001; Sanderson-Smith et al., 2007; Schenone et al., 2000).

Since the binding domains of PAM and hPg were originally defined (Wistedt et al., 1995; Wistedt et al., 1998), a small peptide, VEK30 from PAM_{AP53}, that contains only its *a1*-repeat, as well as VKK38 from PAMNS455, that is composed of both the *a1*- and *a2*-repeats, along with $K2_{hPg}$ have been employed as minimalistic structural models to investigate the essential aspects of the very specific and tight binding of PAM proteins to hPg. The side-chains of residues $R^{17}H^{18}$ and $E^{19}E^{20}$ of VEK30 serve as positive and negative clusters around one turn of an α-helix. The residues are spaced similarly to the α-COOH and ε-NH_2 of a free lysine and fit into the LBS of $K2_{hPg}$. This has been interpreted as an *a1*-located lysine side-chain isostere (RH1) in PAM_{AP53} (Rios-Steiner et al., 2001; Wang et al., 2010b). Similarly, the side-chains of the more extended VKK38, containing residues $R^{30}H^{31}$ and $D^{32}H^{33}D^{34}$, constitute a second *a2*-positioned lysine isostere (RH2) in PAMNS455 (Yuan et al., 2017). We showed previously that VKK38 can accommodate two $K2_{hPg}$ peptides on the VKK38 α-helix, likely on opposite faces of this helix (Yuan et al., 2017).

We aimed to elucidate the roles of each of the two hPg/hPm binding sites in PAM in order to assess their equivalency in the structure and function of PAM, especially since other Pattern D GAS strains are highly substituted in this region. Additionally, some Pattern D GAS isolates only contain one hPg/hPm binding site in the PAM A-domain (the *a2*-repeat), *e.g.*, PAMNS88.2. These PAMs display different hPg acquisition properties than those with two hPg/hPm binding sites (Qiu et al., 2018). Thus, an understanding of the mechanism of binding of hPg to PAM has become an important factor in the study of GAS virulence. In an associated recently submitted paper (Quek et al, submitted for publication), a larger peptide, VEK75, sequentially containing a C-terminal portion of the hypervariable region (HVR)-the full A-domain-and a partial N-terminal portion of the B-domain of PAM_{AP53} (Bhattacharya et al., 2014), in complex with $K2_{hPg}$, has been crystallized and the structure solved, showing that the two binding sites in this PAM_{AP53} peptide can simultaneously bind to $K2_{hPg}$. In order to resolve potential generic issues surrounding the influence of crystal packing forces in determining the final structure, and/or rearrangement of the conformations for optimal crystal formation, and to obtain a more direct observation of the interchain binding interactions in solution, we have additionally determined the solution structure of a VEK50/$K2_{hPg}$ complex, using a functionally similar, but slightly shorter (for ease in assigning NMR chemical shifts), fragment of PAM_{AP53} containing its full A-domain. VEK50 is extended in sequence from VEK30 and VKK38 to more rigorously assess possible exosites in binding. The high equivalency of the studies with a variety of peptides from the A domain of PAM clarifies the binding modality of hPg to PAM_{AP53}.

2. Materials and Methods

2.1. Construction of expression plasmids

The construction of plasmids for peptide and protein expression was accomplished as previously described (Wang et al., 2010b). VEK50, cloned from PAM_{AP53}, and VEK50 mutant peptides, generated by site-directed mismatch mutagenesis with synthetic oligonucleotides, were expressed in *Escherichia coli* BL21 (DE3) cells employing the His_6-tagged-GB1 domain fusion expression system (Wang et al., 2010b). The final constructs contained sequentially from the 5': [ATG initiation codon - purification His_6 tag - GB1 domain for enhanced solubility - 9-residue linker - thrombin cleavage site, LVPR/GS, followed by the VEK peptide]. This cassette was inserted into pET-15b (Novagen) (Wang et al., 2010b). Thus, all peptides cleaved with thrombin possessed an exogenous GS dipeptide at the N-terminus. In addition, a codon for a Tyr was intentionally placed at the C-termini of the VEK peptides for 280 nm absorption properties (Bhattacharya et al., 2014). All plasmid inserts were subjected to full nucleotide sequencing and only those identical to the expected sequences were employed for expression.

2.2. Expression and purification of VEK peptides

The expression of VEK50 peptides was carried out in *E. coli* BL21 using previously published protocols (Wang et al., 2010b). After induction with 0.8 mM isopropyl-1-thio-β-D-galactopyranoside (IPTG), proteins extracted from the cell pellet were loaded onto a Ni^{2+}-Sepharose affinity chromatography column (HisTrap HP; GE Healthcare) at 4° C, washed, and eluted with 60 mM imidazole, pH 8.0. The concentrated eluates were further purified after cleavage with 1000 U of thrombin (ERL). The resulting cleaved fragments were separated using a HisTrap HP affinity column (GE Healthcare). At this step, the flow-through fraction, containing VEK50 peptides, was applied to p-aminobenzamidine agarose (Sigma) to remove thrombin. To prepare ^{15}N- and $^{15}N/^{13}C$-VEK50 samples for NMR experiments, expression and purification were similarly accomplished as described previously (Wang et al., 2010a; Wang et al., 2010b). For uniform labeling, $^{15}NH_4Cl$ (99%, Cambridge Isotope Laboratories) and/or ^{13}C-glucose (99%, Isotec) were used as the sole nitrogen and carbon sources, respectively.

2.3. Expression and purification of $K2_{hPg}$

A triple variant of human $K2_{hPg}$ (C^4G/E^{56} $D/L^{72}Y$) that displays ~5-fold enhanced affinity. without loss of selectivity for PAM, as well as the inability to aggregate through disulfide bonding, compared to WT-$K2_{hPg}$, was expressed in *Pichia pastoris* GS115 cells as described in detail previously (Nilsen et al., 1997; Wang et al., 2010a; Wang et al., 2010b). The tighter binding of this variant allowed separation of $K2_{hPg}$ from unbound components during purification. For uniform ^{15}N- and $^{15}N/^{13}C$-$K2_{hPg}$, the medium employed was ($^{15}NH_4)_2SO_4$ (99%, Cambridge Isotope Laboratories)/^{13}C-glucose (99%; Isotec)/^{13}C-methanol (99%, Isotec). The $K2_{hPg}$ contained seven exogenous residues at the N-terminus of $K2_{hPg}$ (enumerated as −7 to −1) as a necessary result of the construction of the expression plasmid (Nilsen et al., 1997). The final construct is as follows:

$$NH_2 - Y^{-7}VEFSEE\left[C^{+1} - K2_{hPg} - C^{78}\right]AA^{80}$$

The $Y^{-7}VEF$ is from the polylinker site of the plasmid and SEE represents the linker between $K1_{hPg}$ and $K2_{hPg}$ in hPg numbering begins at C^{+} and concludes at C ^{78}

The integrity of all labeled and unlabeled proteins and peptides was determined by MALDI-TOF mass spectrometry on an Autoflex III spectrometer (Bruker Daltonics). For all uniformly-labeled ^{15}N- and $^{13}C/^{15}N$-peptides, single mass peaks were obtained of the correct molecular weights, indicating complete incorporation of the heavy isotopes.

2.4. Extinction coefficients of peptides and proteins

Precise concentrations of the peptides and proteins are required for accurate titrations of the VEK-peptides and $K2_{hPg}$. For this, we directly determined extinction coefficients of all samples at 280 nm. Since the VEK peptides are naturally devoid of aromatic residues, a C-terminal Tyr residue was added at the COOH-termini of these peptides to provide an observable A_{280nm}. Next, we determined the A_{280nm} combined with the refractive indices (RI) on the same samples. The procedure made use of a combination of size exclusion chromatography (SEC), to separate any impurities in the sample, with the column flow-through passed in-line through a 2013variable wavelength detector (VWD), set to monitor UV absorbance at 280 nm, a light scattering detector to ensure that the molar mass of the eluted peak matched that of the peptide of interest, followed by a refractive index detector (RID). The equipment used was an Agilent 1260 infinity II HPLC system with a Wyatt WTC-030S5 (7.8 × 300 mm, 5 μm, 300Å) SEC column coupled to Wyatt Treos II multi-angle (three angles) light scattering (MALS) detector, an Agilent VWD, and a Wyatt Optilab T-Rex RID. The flow path, together with the SEC column, was equilibrated with PBS, pH 7.4. The sample (100 μl) in the same buffer was added to the column *via* an autosampler and passed through the SEC column. Approximately 95% of all samples applied reached the detectors. Since the refractive index increments of the peptides are constant at 0.185 ml/g, the A_{280nm} and RI values allow the extinction coefficient of the sample to be readily calculated (Wen et al., 1997).

The experimental extinction coefficients (ml mg^{-1} cm^{-1}) determined from this approach (compared to those calculated from ExPASY (Gasteiger et al., 2003) are: $K2_{hPg}$ = 2.38 (2.40); VEK50 = 0.20 (0.24); $VEK50^{\Delta RH1}$ = 0.21 (0.25); $VEK50^{\Delta RH2}$ = 0.21 (0.25); hPg (for a positive control) = 1.75 (1.72). In all cases, the experimental extinction coefficients were used for concentration determinations.

2.5. Isothermal titration calorimetry (ITC)

ITC measurements were performed at 25° C on a VP-ITC 200 Microcal calorimeter (Malvern) in 50 mM sodium phosphate, pH 7.4. For VEK50/$K2_{hPg}$ binding, VEK50 peptides (40 μM) was stirred in a cell at ~800 rpm and $K2_{hPg}$ (900 μM) was injected at a rate of 4 μl/s for WT-VEK50 and 2 μl/s for VEK50 mutants with 120 sec equilibration time. Control experiments were performed by titrating $K2_{hPg}$ to buffer instead of VEK peptides.

The integrated heats of interaction were normalized to the molar ratio of VEK50 peptide to $K2_{hPg}$, and the data were fit with Origin-ITC 7.0 software.

2.6. Analytical ultracentrifugation (AUC)

The molecular weights of individual proteins were determined by AUC equilibrium analysis with a Beckman Optima XLI ultracentrifuge. Purified $K2_{hPg}$ (10 μM) and VEK50 peptides (150 μM), at 0.1 – 0.3 μg/ml, were analyzed in 20 mM Tris-Cl/0.1M NaCl, pH 7.4, at 25° C. A_{280nm} data from rotor speeds of 32,000 and 40,000 rpm were recorded every hr until the scans were identical, thus indicating that equilibrium was attained. The partial specific volumes of the VEK50 peptides and $K2_{hPg}$ were calculated from their amino acid sequences using Sednterp (Laue et al., 1992). AUC data were analyzed by the Optima XL-A/XL-I data analysis software (Beckman Coulter), and apparent molecular weights were obtained throughout the concentration gradient generated in the cell (Bhattacharya et al., 2014).

For complexes of $K2_{hPg}$ and each VEK50, the peptides were mixed in a 3:1 molar ratio of $K2_{hPg}$:VEK50 and loaded onto a S75 gel filtration column (GE Healthcare) equilibrated with 20 mM Tris-Cl/0.1 M NaCl, pH 7.4. The column was operated with an AKTA FPLC system at a flow rate of 0.5 ml/min and elution was monitored by A_{280nm}. The complex was resolved from free $K2_{hPg}$ and the first peak to elute was concentrated by membrane filtration (3K-MWCO), and analyzed on the AUC as described above.

2.7. NMR

2.7.a. Data collection—Protein concentrations used for NMR samples of the apo-VEK50 peptides, apo-$K2_{hPg}$, and the VEK50/$K2_{hPg}$ complexes ranged from 0.2 –1.0 mM. Purified samples of the VEK50s and $K2_{hPg}$ were dialyzed against NMR sample buffer (20 mM Bis-Tris-d19/2 μM DSS/5% ^2H_2O/95% H_2O, pH 6.7) prior to NMR measurements. In order to solve the bound-form structures of the VEK50 peptides with $K2_{hPg}$, $^{15}N/^{13}C$-VEK50, $^{15}N/^{13}C$-VEK50[RH1/AA] ($VEK50^{\Delta RH1}$), and $^{15}N/^{13}C$-VEK50[RH2/AA] ($VEK50^{\Delta RH2}$) samples were mixed with unlabeled $K2_{hPg}$ at molar ratios of 1:2, 1:1, and 1:1, respectively.

Data were acquired at 298 K on a Bruker AVANCE 800 spectrometer equipped with a 5-mm triple resonance (TCI, ^1H, ^{13}C, ^{15}N) cryoprobe. Standard triple resonance NMR experiments were used to assign $^{15}N/^{13}C$-labeled VEK50 peptide samples. The following spectra were collected: ^{15}N-HSQC (Kay et al., 1992; Mori et al., 1995), ^{15}N-TOCSY-HSQC (Marion, 1989 #13328} (80 ms mixing time), HNCO/HN(CA)CO (Clubb et al., 1992; Kay et al., 1990), HNCA (Grzesiek and Bax, 1992), HNCACB/CBCA(CO)NH (Grzesiek et al., 1993a; Wittekind and Mueller, 1993), C(CO)NH (Grzesiek et al., 1993b) for the backbone and aliphatic side chain resonance assignments, as well as ^{15}N-NOESY-HSQC (Talluri and Wagner, 1996) and ^{13}C-NOESY-HSQC (Ikura et al., 1990), to collect intramolecular NOE distance constraints for the structure calculations. NMR data were processed using Bruker TopSpin 3.5 software and analyzed using NMRFAM-Sparky (Lee et al., 2009). ^1H chemical shifts were referenced to internal DSS, while ^{13}C and ^{15}N chemical shifts were referenced indirectly to DSS (Markley et al., 1998).

For docking studies, intermolecular distance constraints were determined by $^{15}N/^{13}C$-half-filtered/edited 3D NOESY-^{1}H-$^{15}N/^{13}C$-HSQC experiments (120 ms mixing time), performed on samples of $^{15}N/^{13}C$-VEK50 peptides complexed to unlabeled $K2_{hPg}$, and $^{15}N/^{13}$ hPg C- $K2_{hPg}$ complexed with unlabeled VEK50 peptides. 2D NOESY experiments with ^{15}N- and ^{13}C-filtered in both dimension (120 ms mixing time) were acquired on the same samples under identical conditions as controls.

2.7.b. Structure calculations of VEK50 peptides—The structures of VEK50 peptides in their apo- and bound-forms were first predicted by the CS-ROSETTA program (Shen et al., 2008) based on their residue-specific chemical shifts obtained from the NMR experiments listed above. Next, the structure from the converged results was used as the template, and further refined by Xplor-NIH 2.36 program (Schweiters et al., 2018). Backbone torsion angle (ϕ and ψ) restraints predicted from TALOS-N distance restraints from NOESY spectra, and RDCs were applied in a simulated annealing protocol in the Xplor-NIH program. For each VEK50 peptide, 200 structures were calculated, from which 20 structures with the lowest energy restraint values were further refined with implicit water (Chen et al., 2004). The quality of the structures was analyzed with PROCHECK 3.5.4 (Laskowski et al., 1993) and MolProbity (Chen et al., 2010). Visualization of the structures was performed using the PyMOL program.

2,7,c. Chemical shift perturbations (CSP)—Titrations for binding studies were carried out by recording $^{1}H/^{15}N$-HSQC experiments on ^{15}N-VEK50 peptides (0.2 mM) with increasing molar ratios of unlabeled $K2_{hPg}$. The amide nitrogen and hydrogen CSPs were mapped for each amino acid according to $\sqrt{(\Delta\delta HN)^2 + (\Delta\delta N/6)^2}$, where $\Delta\delta^{HN}$ and $\Delta\delta^{N}$ represent the chemical-shift changes of ^{1}H and ^{15}N atoms between the apo- and bound-forms, respectively (Williamson, 2013). CSP values for $K2_{hPg}$ were collected from reversed-labeled samples of the complexes, *i.e.*, ^{15}N- $K2_{hPg}$ titrated with increasing molar ratios of unlabeled VEK50 peptides.

2.7.d. RDC measurements—Residual dipolar coupling (RDC) measurements were performed on ^{15}N-VEK50, ^{15}N-VEK50$^{\Delta RH1}$, and ^{15}N-VEK50$^{\Delta RH2}$ in their apo-forms and in complexes with unlabeled $K2_{hPg}$ at molar ratios of 1:2, 1:1, and 1:1, respectively. Additionally, ^{15}N-$K2_{hPg}$, complexed with unlabeled mutant VEK50 peptides, was analyzed at a molar ratio of 1:1. In all cases, the concentration of labeled protein ranged from 0.2 mM to 0.5 mM, and the unlabeled protein was present in sufficient excess to ensure that the labeled protein was entirely in the bound state. $^{1}D_{NH}$ RDCs were measured using two-dimensional IPAP[$^{15}N/^{1}H$]HSQC experiments (Ottiger et al., 1998). RDC values for each residue were obtained by taking the difference in the corresponding *J*-splittings measured in magnetically oriented (~10 mg/ml) Pf1 phage and isotropic in H_2O. The magnitudes of the axial component of the tensor, D_a^{NH} (−16.5 Hz) and rhombicity, η (0.45), components of the alignment tensor, were determined based on the NMR structure of VEK30/$K2_{hPg}$ (PDB code:2KJ4) using the DC program (https://spin.niddk.nih.gov/bax/). For CSP and RDC data analyses, sequence-specific backbone ^{15}N-^{1}H assignments for $K2_{hPg}$, published previously (Wang et al., 2010a), were used.

2.7.e. Restraint-based docking of the VEK50/K2$_{hPg}$ complex—Restraint-based docking calculations for the complexes of VEK50 peptides with **K2$_{hPg}$** were performed on the HADDOCK web server (van Zundert et al., 2016) and the Xplor-NIH program. The topologies and starting structural coordinate files for input into HADDOCK were generated from the refined NMR structures. For generation of ambiguous interaction restraints, residues $R^{17}H^{18}$ of VEK50$^{\Delta RH2}$ and residues $R^{30}H^{31}$ of VEK50$^{\Delta RH1}$ that are directly involved in interaction with K2$_{hPg}$ were defined as active-site residues, and residues with significantly different CSP values ($^{\Delta}\delta$ > 0.2 ppm) were defined as passive residues. For K2$_{hPg}$, residues exhibiting CSP values larger than 0.1 ppm were defined as active residues, i.e. the ones at binding site. The passive residues of K2$_{hPg}$ were automatically picked by HADDOCK server program based on its 3D structure. RDC orientation constraints and intermolecular NOEs from VEK50 peptides and K2$_{hPg}$ were used as unambiguous restraints for structure calculation to obtain the complex of VEK50$^{\Delta RH2}$/K2$_{hPg}$ and VEK50 $^{\Delta RH1}$/ K2$_{hPg}$ at molar ratios of 1:1. Segments of VEK50 peptides and K2$_{hPg}$ that constituted these active and passive residues, plus two sequential residues on either side of the active and passive residues, were kept semiflexible during the docking steps. N- and C-residues of VEK50 peptides (residues 1–8 and 48–50) were kept flexible throughout the docking. The alignment tensor was calculated using the DC program with default parameters for singular value decomposition (SVD) fitting (https://spin.niddk.nih.gov/bax/). Intervector projection angle restraints for VEAN were generated with the python script provided in HADDOCK.

The simulated structure model of the VEK50/K2$_{hPg}$ complex at a molar ratio of 1:2 was obtained from HADDOCK combined with the CSP data from NMR ^{15}N-HSQC titration experiments for VEK50/K2$_{hPg}$, along with previous results for VEK30/K2$_{hPg}$ (Wang et al., 2010b). The dihedral angle restraints for the bound-form of K2$_{hPg}$ and VEK50 predicted from TALOS-N were also included in HADDOCK calculation. For purposes of docking, intermolecular NOEs and RDCs of K2$_{hPg}$ bound at $R^{17}H^{18}$ of VEK50$^{\Delta RH2}$, and K2$_{hPg}$ bound at $R^{30}H^{31}$ of VEK50$^{\Delta RH1}$ were used to define the relative positions of the two K2$_{hPg}$ molecules in their complexes with VEK50. The structural models were clustered and the best model with the highest HADDOCK score was selected to present the structure of the complex. The statistical data for the structures derived from HADDOCK are listed in Supporting Information Table S1.

2.8. Data deposition

The coordinates of the calculated structural ensembles for the bound-form of VEK50, as well as the structural ensembles for the complex of K2$_{hPg}$ with VEK50$^{\Delta RH1}$, and K2$_{hPg}$ with VEK50$^{\Delta RH2}$, have been deposited in the Protein Data Bank with accession codes 6OQ9, 6OQJ, and 6OQK respectively. Chemical shift assignments for the VEK50 peptides in complex with K2$_{hPg}$ and the corresponding experimental restraints used in the structure calculation have been deposited in the BioMagResBank with accession numbers 30603, 30605, and 30606, respectively.

3. Results

3.1. Binding stoichiometry of the VEK50 peptides to $K2_{hPg}$

3.1.a. ITC titrations—VEK50 is a truncated peptide of PAM_{AP53} that sequentially includes: [the C-terminus of the hypervariable region (HVR) - the entire A-domain, including its component *a1a2*-repeats and the N-terminus of the flexible B-domain]. This peptide begins at V^{97} of PAM_{AP53}, which is residue-1 in VEK50 (Table 1). To quantitate binding of VEK50 to $K2_{hPg}$, ITC measurements were employed. The heats of binding were measured at 25° C as a function of molar ratio of $K2_{hPg}$ to VEK50. As shown in Figure 1A, the binding isotherm is best-fit by a molar stoichiometry of 2:1 for $K2_{hPg}$:VEK50, with an average K_d value of 9 nM. In order to identify the binding properties of the RH motifs separately, two mutant peptides, $VEK50^{\Delta RH1}$ and $VEK50^{\Delta RH2}$, were designed by separately replacing RH1 ($R^{17}H^{18}$) or RH2 ($R^{30}H^{31}$) in VEK50 (Table 1) with two Ala residues. This yields peptides, $VEK50^{\Delta RH1}$ and $VEK50^{\Delta RH2}$, respectively. Using these peptides in the titrations, a molar binding stoichiometry of 1:1 was observed for $K2_{hPg}$/$VEK50^{\Delta RH1}$, with a K_d of 9 ± 2 nM (Figure 1B) and for $K2_{hPg}$/$VEK50^{\Delta RH2}$ of 42 ± 4 nM was best-fit to the data (Figure 1C). These results confirmed that the RH motifs are the active-site residues that are directly involved in the binding to $K2_{hPg}$. The binding affinities of these two mutants also show that $K2_{hPg}$ binds more tightly to RH2 than RH1.

3.1.b. AUC analyses—The binding stoichiometry between VEK50 peptides and $K2_{hPg}$ was further assessed by determining the molecular masses of the complexes of VEK50/$K2_{hPg}$ using analytical AUC. The complexes of VEK50 peptides with $K2_{hPg}$ were prepared using three different initial concentrations of $K2_{hPg}$ (13 μM, 19 μM, and 25 μM) added to VEK50 (5 μM, 7.5 μM, and 10 μM), each representing a ~2.5-fold molar excess of $K2_{hPg}$/VEK50 at different total concentrations of the complex. The complexes were separated from the nonbound materials by gel filtration. The theoretical molecular mass of $K2_{hPg}$ is calculated to be 10,151 Da, that of VEK50 is calculated as 6,159, and, for the two mutant VEK50 peptides, the calculated molecular masses are 6,008 Da, all in agreement with the MALDI data listed in Table 2. From the AUC data of Table 2, it is clear that a 2:1 molar complex of $K2_{hPg}$/VEK50 is found, whereas for the two mutant complexes, *viz.*, $VEK50^{\Delta RH1}$/$K2_{hPg}$ and $VEK50^{\Delta RH2}$/$K2_{hPg}$, the molecular masses of the isolated complexes corresponded to a 1:1 molar stoichiometry (Table 2). In all cases, a single molecular mass species was found throughout the concentration gradient in the centrifugation cell. This single species that exists over a wide concentration range supports the ITC data showing that very tight binding occurs.

3.1.c HSQC titrations of VEK50 peptides to $K2_{hPg}$—$^{1}H/^{15}N$-HSQC experiments were recorded on ^{15}N-VEK50 peptides with increasing unlabeled $K2_{hPg}$ at 1:0.5, 1:1, 1:1.5, 1:2.0, and 1:2.5 molar ratios of VEK50:$K2_{hPg}$ respectively (Figure 2A–D; Supporting information Figure S1). During the titrations the chemical shifts of residues at the N- and C-terminii, viz., V^{1}-K^{3} and D^{49}-Y^{50}, respectively, change only slightly and only one peak for each residue is observed in NMR spectra. This suggests that these residues experience fast exchange (Figure 2A). However, the amide resonances of most residues in VEK50 peptides shift significantly and start to appear at two locations. As one example of the data, when

$K2_{hPg}$ was titrated to 1:0.5 ratio, residue A^{48} in VEK50 (Figure 2B), -VEK50$^{\Delta RH1}$ (Figure 2C), and -VEK50$^{\Delta RH2}$ (Figure 2D) showed two peaks, corresponding to the amide resonances in the apo- and bound-forms. respectively. After a 1:1 molar ratio was reached, all of the amide resonances in VEK50$^{\Delta RH1}$ and VEK50$^{\Delta RH2}$ are shifted to the positions of the bound forms, as exemplified by A^{48} (yellow) in Figure 2C, D. These residues remained at the same locations when additional unlabeled $K2_{hPg}$ was added to the system. Meanwhile, amide resonances of some residues in VEK50 show three peaks indicating the existence of a mixture containing apo-, 1:1, and 1:2 molar complexes of VEK50 to $K2_{hPg}$. These residues are located in both the *a1*- and *a2*-repeats, suggesting that $K2_{hPg}$ similarly binds to each of these two motifs. The amide resonances were continually shifted until a 1:2 molar ratio of VEK50/$K2_{hPg}$ was reached, as exemplified by A^{48} (colored blue) in Figure 2B. These results further confirm that the VEK50 peptide within PAM_{AP53} contains two binding sites for $K2_{hPg}$ and that the binding is mediated by RH motifs in each repeat of the *a1a2* domain. For each of the two VEK50 mutants, a 1:1 binding stoichiometry is also confirmed.

On the basis of these titration experiments, the combined CSPs for the three VEK50 peptides are summarized in Figure 2 (E–G). These data show that residues displaying large chemical shift perturbations upon binding to $K2_{hPg}$ are not limited to $R^{17}H^{18}$ in the *a1*-repeat and R $^{30}H^{31}$ in the *a2*-repeat, but also occur in other residues in that region, demonstrating the existence of probable exosites identified using this longer peptide from PAM_{AP53}. The results also demonstrate that conformational transitions occur in VEK50 peptides upon binding to $K2_{hPg}$. For example, the residues in VEK50$^{\Delta RH1}$ showing most significant CSPs are in the RH2 binding region, *i.e.*, residues L^{26}-K^{36} (Figure 2E). In the mutant VEK50$^{\Delta RH2}$ the chemical shift changes were found between residue A^{8} to E^{20}, which consists of the RH1 binding motif (Figure 2F). Since WT-VEK50 contains both the RH1 and RH2 binding motifs, most of the residues in VEK50, except those in the N-, and C-terminal regions, show significant chemical shift changes at most locations upon binding to $K2_{hPg}$ (Figure 2D).

In addition, ^{1}H-^{2}H exchange experiments were performed for three VEK50 peptides in the apo-forms and in the complex with $K2_{hpg}$ by dissolving lyophilized sample in $^{2}H_2O$, followed by temporal acquisition of HSQC spectra. For the apo-form peptides and the complex of two mutant VEK50 peptides with $K2_{hPg}$, amide resonances disappear during the first 20 min period. Meanwhile, amide resonances of some residues in the WT-VEK50/$K2_{hPg}$ complex remain, and those from residues L^{26}, K^{27}, and E^{29} are still detectable after 20 hr (Figure 3), indicating that these residues become less exposed to solvent upon VEK50 binding with two $K2_{hPg}$ molecules.

3.2. Binding sites in K2hPg for a1- and a2-repeats

3.2.a. Chemical shift differences show that RH1 and RH2 bind to the same LBS of $K2_{hPg}$—Chemical shift changes in $K2_{hPg}$ are also ligand-induced, and primarily found in the LBS (Figure 4). The binding of $K2_{hPg}$ to either wild-type VEK50 or its mutant peptides, VEK50$^{\Delta RH1}$ and VEK50$^{\Delta RH2}$, is detected in HSQC spectra by monitoring changes in $^{1}H/^{15}N$ chemical shifts from ^{15}N-labeled $K2_{hPg}$ as a function of the concentration of VEK50 peptides (Supporting Information Figure S2). Three segments in

$K2_{hPg}$, *viz.*, G^{34}-K^{46}, D^{54}-W^{60}, and K^{68}-E^{71}, exhibit the most dramatic CSPs upon binding to VEK50 peptides, suggesting these are binding residues in $K2_{hPg}$ (Figure 4). Several residues in these regions, such as D^{54} and R^{55}, show weak or very broad signals in the apo-form of $K2_{hPg}$, but shift to a new position in the bound-form (Supporting Information Figure S2). These results are consistent with previous studies for the $K2_{hPg}$/VEK30 complex (Wang et al., 2010b), but, additional residues in $K2_{hPg}$ are affected when $K2_{hPg}$ binds to the larger VEK50 peptides, further indicating available exosite interactions. The CSP data also suggest that $K2_{hPg}$ uses the same domain for binding to either VEK50$^{\Delta RH1}$ or VEK50$^{\Delta RH2}$ (Figure 4A,B). When three HSQC spectra of $K2_{hPg}$ bound to VEK50 and two mutant peptides were overlaid (Supporting Information Figure S2C), most of peaks appeared at the same chemical shifts. However, in the HSQC spectrum of $K2_{hPg}$ bound to VEK50, the residues with larger CSP always show at two locations with different peak intensities. For examples, D^{54}, L^{57}, and W^{60} of $K2_{hPg}$ have two fresonance signals corresponding to two $K2_{hPg}$ molecules bound to RH1 or RH2 of VEK50 respectively (Figure 4C). Notably, the signals from $K2_{hPg}$ bound to RH2 show a 3–5-fold stronger peak intensities, suggesting that in the presence of excess of VEK50, RH2 is more favorable for $K2_{hPg}$ binding. This is also consistent with the ITC results for two mutant VEK50 peptides. Thus, the difference of K_d values observed from the mutants truly represents the stronger binding ability of the RH2 site in the WT-VEK50, which is not affected by the steric crowding of two $K2_{hPg}$ molecules in the complex. Slight differences are also observed in the segment comprising residues G^{6} - N^{8}, which is close to the flexible N-terminus, therefore, the differences are likely not directly related to ligand binding.

3.2.b. The binding interface in $K2_{hPg}$ for RH1 and RH2—Although only one binding domain is detected in $K2_{hPg}$ by NMR titration, the binding interface formed between $K2_{hPg}$ and the *a1*- or *a2*-repeat in two mutant VEK50 peptides is somewhat different. The differences are observed from the NMR solution structures of $K2_{hPg}$ in the complex with the two mutant peptides, which are refined by residual dipolar coupling (RDC) data. A total of 63 amide RDCs ($^{1}D_{NH}$) from ^{15}N-$K2_{hPg}$/unlabeled VEK50$^{\Delta RH1}$ and 60 amide RDCs ($^{1}D_{NH}$) from ^{15}N-$K2_{hPg}$/unlabeled VEK50$^{\Delta RH2}$ were obtained from RDC measurements using 2D IPAP- HSQC (Supporting information Figures S3 A, B). The RDC data obtained from these two complexes were fitted to the solution structure of the bound-form of $K2_{hPg}$ in complex with VEK30 (PDB code: 2kj4) (Wang et al., 2010b), which contains only the RH1 binding motif. It was found that residues on N- and C-termini exhibit larger differences (>5 Hz) between the calculated and observed RDCs ($^{1}D_{NH}$). The residues in the ligand binding region, such as D^{54}-L^{57} and W^{60}, which show differences in the sign and intensity of the absolute RDC values in Figures S3 A,B, also exhibit larger differences (>3 Hz) when the experimental RDCs are fitted to the bound-form of $K2_{hPg}$ (Figures S3 C,D). Therefore, we used these experimental RDCs to refine the bound-form of $K2_{hPg}$ with VEK30 in order to provide more precise structures for $K2_{hPg}$ with VEK50 peptides. As depicted in Figure 4D, the binding region (colored red and green) in the two complexes can be overlaid with a RMSD of 1.30 Å, while the rest of $K2_{hPg}$, except the residues at the flexible N- and C-termini, which are exogenous to $K2_{hPg}$, have a RMSD of 0.6 Å. Additionally, the binding region, D^{54}-P^{59}, has a more open conformation in the complex with VEK50$^{\Delta RH1}$.

3.3. Changes in solution structure of VEK50 peptides upon binding to $K2_{hPg}$

3.3.a. Apo-structures of three VEK50 peptides—The solution structures of VEK50 peptides in their apo-forms were calculated based om NMR data (Figure 5). The residues in the N-terminal region, *viz.*, V^1 - D^7, and in the C-terminal region, *viz.*, D^{49} - Y^{50}, have only sequential connectivities, suggesting that these regions exist as coils. In apo-VEK50, three short α-helical segments, *viz.*, A^8 - K^{14}, E^{22} - R^{30}, and K^{37} - K^{46}, are connected through two flexible loops, which contain the RH1 and RH2 motifs (Figure 5A). The overall structures of two mutant peptides are very similar to that of WT-VEK50, although one of the RH groups has been replaced by Ala-Ala residues. The RH2 group of $VEK50^{\Delta RH1}$ (Figure 5B) and the RH1 group in $VEK50^{\Delta RH2}$ are also in the loop regions in the apo forms (Figure 5C).

3.3.b. Bound structures of three VEK50 peptides—The binding regions, RH1 and RH2, in VEK50 undergo significant structural changes and become more rigid upon its binding to $K2_{hPg}$. Thus, as shown in Figure 5D, the helical segment from residue A^6 - D^{32} in VEK50 is formed and two RH groups ($R^{17}H^{18}$ and $R^{30}H^{31}$) are positioned on opposite faces of the helix. The mutant peptides also exhibit conformational changes but those changes mainly occur at the binding regions (Figure 5E,F). The alanine replacements in $VEK50^{\Delta RH1}$ enhance the rigidity of the region consisting of A^6 - E^{19} in the apo-form. However, the conformation of this region does not significantly change and remains bent in the complex. The conformation of $VEK50^{\Delta RH2}$ exhibits high similarity to WT-VEK50 in its bound form, especially the RH1 binding regions.

Residual dipolar coupling (RDC) data provide additional structural and dynamic information in a μsec timescale for the bound-form VEK50 peptides. The plot of ^1H-^{15}N RDCs as a function of the residue number (Figure 2H–J) confirm that most of the residues in the *a1a2*-repeat of VEK50 have RDC absolute values above 5 Hz, while the residues at N- and C-terminal are flexibly disordered, presenting significantly smaller RDCs (< 3Hz) (Figure 2H). The plot of the RDCs for $VEK50^{\Delta RH1}$ show that the residues presenting large RDCs are not limited to those in the binding region, *i.e.*, the *a2*-repeats (Figure 2I), whereas the residues in *a1*-repeat of $VEK50^{\Delta RH2}$ exhibit significantly larger RDCs (Figure 2J), consistent with the more rigid structure formed upon binding.

All three peptides in the bound form contain a helical segment (L^{23} - E^{29}) between the two RH motifs. The helical feature gained in the bound form of these peptides fades at the end of the *a2*-repeat. Residues 1–7 at the N-terminus and residues 49–50 at the C-terminus are flexible and show sharp resonance signals in HSQC spectra. But residues 44–48 are always present at two locations in HSQC spectra, indicating that this fragment is in slow exchange between locally different structures in the bound form.

3.4. HADDOCK calculated structural models of the $K2_{hPg}$/VEK50 complexes

In this study, we present a structural basis of the binding of VEK50, an active fragment of PAM_{AP53}, to $K2_{hPg}$ and provide evidence for the high affinity and specificity of this peptide. From a previous study of the VEK30/$K2_{hPg}$ complex (Wang et al., 2010b), the hydrophobic groove in $K2_{hPg}$ formed by Y^{35}, F^{40}, W^{60}, W^{70}, and Y^{72} in combination with the anionic

center of D ^{54} and D^{56}, comprised the binding site of $K2_{hPg}$/RH1. These same residues in $K2_{hPg}$ also exhibit significant chemical shift perturbations upon its binding to either the *a1*-repeat in VEK50$^{\Delta RH2}$ or *a2*-repeat in VEK50$^{\Delta RH1}$ (Figure 4), suggesting that there is only one potential interaction site for $K2_{hPg}$ in the complex with VEK50 peptides.

For the VEK50 peptides, the active-site residues, which directly participate in binding, were assigned based on the mutations studied previously and the CSPs observed from NMR titrations in this study (Figure 2). It is noted that both VEK50$^{\Delta RH1}$ and VEK50$^{\Delta RH2}$ contain the complete *a1*- and *a2*-repeats, except that one of the RH groups has been replaced by Ala-Ala, thus inactivating the $K2_{hPg}$ binding site in each repeat. Thus, only the fragment having the intact RH motif exhibits large CSPs upon the binding to $K2_{hPg}$ (Figure 2F, G). This further confirms that the RH motifs are critical residues for tight $K2_{hPg}$ binding. Other residues, *i.e.*, 10–22 in VEK50$^{\Delta RH1}$ and 24–34 in VEK50$^{\Delta RH2}$, with dramatic chemical shift changes, were also directly related to binding, and were defined as passive residues for docking calculations.

The interface of VEK50 peptides and $K2_{hPg}$ was also identified by the intermolecular NOEs between $^{13}C/^{15}N$-$K2_{hPg}$ and unlabeled VEK50 peptides, or $^{13}C/^{15}N$-labeled VEK50s and unlabeled $K2_{hPg}$. For example, methyl resonances from L^{26} of VEK50$^{\Delta RH1}$ exhibited NOEs to residues H^{33}, G^{34}, Y^{35}, and I^{36} of $K2_{hPg}$. Similar NOEs were also observed form L^{13} of VEK50$^{\Delta RH2}$ with corresponding residues in $K2_{hPg}$, suggesting that these residues are in close contact with each other. Using $^{13}C/^{15}N$-filtered, $^{13}C/^{15}N$-edited NOESY-HSQC experiments, 12 and 14 intermolecular NOEs between $K2_{hPg}$/VEK50$^{\Delta RH1}$ and $K2_{hPg}$/VEK50$^{\Delta RH2}$ were observed, respectively, and used as unambiguous distance restraints.

In addition to these distance restraints, RDC data collected from ^{15}N-labeled $K2_{hPg}$ (Figure 4C) and ^{15}N-labeled VEK50 peptides (Figure 2 H–J) in the corresponding complex were included to provide the orientation restraints for docking. When the complex samples were oriented in Pf1 phage medium, no noticeable structural perturbations were observed. A total of 90 and 93 RDCs ($^1D_{NH}$) obtained from the complexes of VEK50$^{\Delta RH1}$/$K2_{hPg}$, and that of VEK50$^{\Delta RH2}$/$K2_{hPg}$, respectively, were applied as orientation restraints in docking. The resulting structures calculated in HADDOCK showed no distance violations and only residues in the mobile N-terminal and the C-terminal regions in $K2_{hPg}$ and VEK50 peptides show RDC outliners (>3 Hz).

Previous work has shown that the LBS of $K2_{hPg}$ contains an anionic center that interacts with positive side-chains of the pseudo-lysine ligand. In the modeled structures of the pseudo-lysine binding sites, the anionic center of $K2_{hPg}$ (D^{54}, D^{56}) is involved in electrostatic interactions with side-chains of residues, K^{14}, R^{17}, and H^{18} in the *a1*-repeat (Figure 6A) and K^{27}, R^{30} and H^{31} in the *a2*-repeat (Figure 6B). In these structural clusters, hydrogen bonds can also form between the side-chains of these same residues in the *a1*- or *a2*-repeat with carbonyl groups of D^{54} and D^{56} in $K2_{hPg}$. Meanwhile, in VEK50$^{\Delta RH2}$, acidic residues D^9 of the *a1*-repeat and E^{20} of the *a2*- repeat are within close contact distances with basic residues R^{55} and R^{69} of $K2_{hPg}$, respectively (Figure 6A). Although VEK50$^{\Delta RH1}$ only contains one binding motif, *viz.*, RH2, the acidic residue, D^9, and basic residues, R^{12} and K^{14} in the *a1*-repeat are all present in this mutant peptide. Since this region

is structured as a bent helical fragment, these residues could act as exosites through electrostatic interactions with $K2_{hPg}$ as illustrated between R^{12} of $VEK50^{\Delta RH1}$ and D^{54} of $K2_{hPg}$ (Figure 6B). Additionally, D^{34} in the *a2*-repeat of $VEK50^{\Delta RH1}$ forms an H-bond with the side-chain of R^{69} of $K2_{hPg}$. Overall, more electrostatic interactions were found between $VEK50^{\Delta RH1}$ and $K2_{hPg}$.

To dock two $K2_{hPg}$ molecules onto VEK50, we used the multi-body interface module on the HADDOCK 2.2 web server. As described earlier, a semi-flexible mode of docking was performed, where the side-chains of the active and passive residues are designated as flexible. The bound-form of VEK50 was determined by NMR (Figure 5D), and the bound-form $K2_{hPg}$ was refined using RDCs. At least, 24 intermolecular NOEs collected from $VEK50^{\Delta RH1}/K2_{hPg}$ and $VEK50^{\Delta RH2}/K2_{hPg}$ were used to define each binding interface in VEK50 with $K2_{hPg}$. The resulting structural model using 20 of the lowest energy structures of VEK50:$K2_{hPg}$ at a molar ratio of 1:2 is shown in Figure 6C. In order to validate the HADDOCK-calculated structures, the observed RDCs of VEK50 were compared with predicted RDCs based on the model and they correlated well with a low Q-factor of 0.5 (Supporting information Figure S4). In these binding models, no further major conformational changes were observed for the NMR-determined bound structures of either VEK50 or $K2_{hPg}$. The bound-form of VEK50 exists as an α-helix between residue D^{7}-D^{34}, while two $K2_{hPg}$ molecules were bound to opposite faces of the helix. Since both of the *a1*- and *a2*-repeats of VEK50 became more structured, these two fragments interact with $K2_{hPg}$ in a very similar manner. For example, the H-bond of R^{17} and R^{30} in VEK50 with the LSB of $K2_{hPg}$ can be consistently formed in the simulated structure model. The interactions identified from this structural model are consistent with the observation from NMR experiments, in which the residues in the $K2_{hPg}$ bound to RH2 always show stronger resonance signals. Additionally, L^{26} and K^{27} of VEK50 are located in the middle of the helix, are buried in the contact surface of the *a2*-repeat and $K2_{hPg}$. This finding is consistent with their slower $^{1}H/^{2}H$ exchange rate when present in complexes with $K2_{hPg}$.

Thus, from these docking calculations, we conclude that two RH motifs have separate clusters to form the required pseudo-lysine ligand that interacts with the LBS of $K2_{hPg}$. RH1 (R^{17}-H^{18}) in the *a1*-repeat combines with D^{9}, K^{14}, and E^{20} with to form the lysine isostere in $VEK50^{\Delta RH2}$, while RH2 (R^{30}-H^{31}) has another group of residues, including E^{24}, K^{27}, and D^{34} to form its own lysine isostere in $VEK50^{\Delta RH1}$.

4. Discussion

The ubiquitous high copy number surface M-protein of GAS, encoded by the *emm* gene, is a major virulence factor in the pathogenesis of these bacteria, primarily due to its ability to protect against various human host innate responses to infection. Further, the ability of M-proteins to interact with host cells and host proteins confers unique properties to the bacterial cells that allow their invasion and dissemination. There are more than 250 serotypes of M-proteins, primarily identified by the highly variable 5'-nucleotide sequences of the *emm* gene, and at least five subfamily patterns of M and M-like proteins (A-E), revealed by nucleotide sequences of the more conserved 3'-nucleotide sequences encoding peptidoglycan spanning domains of these proteins (Bessen, 2016). These serotypes and

pattern types are of epidemiological value through allowing characterization of infectious breakouts and their possible consequences.

The mature form of M-protein is covalently anchored to the bacterial cell wall at the C-terminus of the protein *via* a typical sortase A-catalyzed linkage. This leaves the N-terminal region of the elongated M-protein to protrude through the GAS outer capsule to interact with host proteins. The sequence variety at the N-termini of M-proteins allows different types of interactions with the host to occur, and there are further differences depending on the serotype of the M-protein. For example, complement-mediated opsonization inhibitors, *e.g.*, C4BP and Factor H, interact with the N-terminal hypervariable regions (HVR) of some *emm*-expressed M-proteins of Patterns A-C and E GAS strains (Buffalo et al., 2016; Gustafsson et al., 2013), and in this manner inhibit opsonization of the bacteria. These same complement inhibitors do not bind to the *emm* gene product (PAM) of Pattern D strains, but do functionally interact with other M-like proteins of these strains, *e.g.*, Enn and Fba, each present along with PAM in the multiple gene activator (*mga)* regulon, and thereby perform this same function (Agrahari et al., 2013; Liang et al., 2013).

Our major interest in GAS-host interactions is centered in the important hemostasis/inflammation responses to GAS infections. Some Pattern A-C strains of GAS interact with fibrinogen in their centralized B-domain (Glinton et al., 2017) and in this way provide anti-opsonic activity to the microorganism (Courtney et al., 2006; Whitnack and Beachey, 1982). All pattern D strains of M-proteins, *e.g.*, PAM from strain AP53, are unique in their ability to bind hPg tightly and directly to their N-terminal A-domains, with profound consequences to their virulence. Activation of hPg to hPm on the GAS surface by GAS-secreted SK2b generates a surface bound protease, hPm, that can aid dissemination in the host by digesting extracellular matrix proteins and cellular epithelial and endothelial tight junctions through this new proteolytic front.

Pattern D M-proteins exist as elongated fibrous proteins, which, at least in solution, have been identified as irregular weakly associated helical coiled-coils (Ghosh, 2011; McNamara et al., 2008; Qiu et al., 2019; Stewart et al., 2016). The COOH-terminal C- and D-domains of PAM that are present close to the GAS capsule, are primarily responsible for dimerization, with large irregularities in the PAM NH_2-terminal HVR-, A-, and B-domains. These irregularities, also seen in coiled-coil proteins such as tropomyosin (Nitanai et al., 2007), appear to allow binding of fibrinogen to B-domains of some M-proteins (McNamara et al., 2008), and thus are of functional significance.

A critical interaction in survival and virulence of Pattern D strains of GAS is the binding of hPg to PAM (Sun et al., 2004) and our work has focused on the nature of this interaction as shown in numerous published studies. The question addressed in this manuscript is the relevance to binding of each of the two adjacent hPg binding sites in the A-domain of PAM. We have employed reductionist approaches in these studies by utilizing peptide secondary structural stretches of PAM, along with the PAM binding K2 domain of hPg. Since PAM is composed solely of secondary structure, with no observed tertiary structure, and $K2_{hPg}$ is an independent domain in hPg (Castellino et al., 1981), this approach should isolate intact

binding sites to allow us to examine the properties of each of the regions of interest in these proteins.

In previous studies using X-ray crystallography (PDB code 1I5K) (Rios-Steiner et al., 2001) and NMR (PDB code 2KJ4) (Wang et al., 2010b), very similar structural models of the $K2_{hPg}$/VEK30 complex have been proposed. The solved structures suggest that there are two interaction clusters formed in the complex. The first is the anionic center of the LBS of $K2_{hPg}$ formed by residues D^{54} and E/D^{56}, which interact with a cationic cluster of side-chains, *viz.*, K^{14}, R^{17}, and H^{18} of VEK30. The second is the cationic locus of the $K2_{hPg}$ binding pocket, R^{69} which forms a salt-bridge with E^{20} of VEK30. The role of each residue in the *a1*-repeat to the binding to $K2_{hPg}$ has been investigated by a variety of mutants, but less has been done for the *a2*-repeat. From our current study, the interactions between residues K^{27}, R^{30}, and H^{31} in the *a2*-repeat act as K^{14}, R^{17}, and H^{18} in the *a1*-repeat. The interactions between the LBS of $K2_{hPg}$ and K^{14}, R^{17}, H^{18}, and E^{20} play major roles in forming a rigid helical structure in the *a1*-repeat. In the bound form of VEK50, RH1 is in the middle of a rigid helical region from the N-terminal of *a1* (D^{7}) to the C-terminal of *a2* (D^{32}), while RH2 is close to the flexible C-terminal of *a2*-repeat. Although both H^{18} in *a1* and H^{31} in *a2* have close contact with the residues of LBS, the H-bond between these two His residues and the LBS are not observed in all models. Meanwhile, the H-bond of R^{17} and R^{30} with the LBS of $K2_{hPg}$ can be consistently formed in all of the lowest energy simulated structures.

VEK50 is a truncated peptide from PAM_{AP53}, which contains both the *a1*- and *a2*-repeats. The replacement of either RH1 or RH2 by Ala-Ala slightly changes the binding affinity of mutant VEK50 peptides to $K2_{hPg}$. The differences observed from their binding affinities to $K2_{hPg}$ are related to the secondary structure of these truncated peptides. VEK50 can bind with $K2_{hPg}$ on the *a1*- and/or *a2*-repeats, while its mutants can only bind using either *a1* or *a2*. As discussed above, the *a2*-repeat has more interactions than the *a1*-repeat with the LBS in $K2_{hPg}$. Thus, compared to $VEK50^{\Delta RH2}$, $VEK50^{\Delta RH1}$ binds to $K2_{hPg}$ tighter *via* its complete *a2*-repeat. As shown in the apo-forms, two RH binding motifs are located in flexible regions in apo-VEK50 and become rigid in the bound-form to obtain complete interactions. The interactions between the LBS of $K2_{hPg}$ and K^{14}, R^{17}, H^{18}, and E^{20} play the major roles in forming a rigid helical structure in the *a1*-repeat. When the RH1 is inactivated by Ala-Ala substitutions, residues in the *a1*-repeat remain as a flexible loop. The selective inactivation of RH2 results in a peptide that can only use its *a1*-repeat to bind to LBS in $K2_{hPg}$. Similarly, this *a1*-repeat alone appears to have fewer interactions with $K2_{hPg}$ compared to the *a2*-repeat. Therefore, $VEK50^{\Delta RH1}$ has a slightly higher affinity than $VEK50^{\Delta RH2}$ for $K2_{hPg}$.

Further affirmation that the entire hPg binding ability is contained within the A-domain of PAM-type M-proteins is evidenced by studies with another class of M-protein, M1 from a Pattern A GAS strain. M1 does not directly interact with hPg, but instead tightly binds to fibrinogen *via* its B-domain. We replaced the entire B-domain of M1 with the A domain of PAM_{AP53}. This mutated M1 no longer interacted with fibrinogen but interacted with hPg nearly identically to PAM_{AP53} (Chandrahas et al., 2015). These results affirm that the *a1a2* module in PAM proteins presents the complete epitope with regard to hPg binding, whereas

effects from other domains in PAM are of little influence in this regard. In the wider scope, we suggest that the domains of M-proteins have evolved independently and have been incorporated into other M-proteins by recombination to generate new GAS strains with advantages for their survival against the immune responses of the host (Bao et al., 2016a; Bao et al., 2016b). The variability of M-proteins, that are relatively rapidly genetically adapted to survive in various host human niches, lies at the basis of the numerous serotypes of GAS that are singularly directed to humans, who cannot evolve as rapidly to combat these bacteria. In addition, the ability of GAS to undergo rapid genetic adaptation is detrimental to M-protein-directed vaccines to combat these infections.

5. Conclusions

Group A *Streptococcus* (GAS) is a bacterial pathogen unique in its remarkable ability to exploit a range of cellular and tissue environments to establish colonization and progress to a wide spectrum of disease states in the human host. A major determinant of GAS host tropism and virulence is the M- and M-like protein (PAM), expressed on the surface of all GAS strains. M-protein forms have evolved to serve highly specialized roles in GAS survival, including its specific ability to recruit and activate hPg. In this report, we provide a detailed structural view of the VEK50/$K2_{hPg}$ complex, a reductionist approach to understanding the nature of the PAM/hPg complex, that offers insights at the molecular scale for the binding mechanism of PAM to hPg. Broadly considered, our findings suggest that the domains of M-proteins have likely been exchanged through horizontal recombination events and independently further evolved in order that emerging GAS strains optimize survival advantages against the host immune response (Bao et al., 2016a; Bao et al., 2016b). The ability of GAS to utilize multiple genetic mechanisms to produce highly variable M-protein forms that successfully allow GAS to adapt to survive in various host human niches, lies at the basis of the numerous serotypes of GAS that are singularly directed to humans, who cannot evolve as rapidly or as specifically to combat these bacteria. Studies aimed at elucidating the mechanistic details of how GAS virulence determinants, such as PAM, engage host targets will provide future insights into improved anti-virulence strategies as well as alternative approaches to improve current vaccine strategies against GAS.

Supplementary Material

Refer to Web version on PubMed Central for supplementary material.

Funding

This work was supported by National Institutes of Health Grant HL013423.

Abbreviations used:

GAS	Group A *Streptococcus pyogenes*
hPm	human plasmin
hPg	human plasminogen

$K2_{hPg}$	kringle 2 domain of human plasminogen
LBS	lysine binding site
PAM	plasminogen-binding group A streptococcal M-like protein
SPR	surface plasmon resonance
CSP	chemical shift perturbation

REFERENCES

Agrahari G, Liang Z, Mayfield JA, Balsara RD, Ploplis VA, Castellino FJ, 2013 Complement-mediated opsonization of invasive Group A Streptococcus pyogenes strain AP53 is regulated by the bacterial two-component cluster of virulence responder/sensor (CovRS) system. J. Biol. Chem 288, 27494–27504. [PubMed: 23928307]

Bao YJ, Shapiro BJ, Lee SW, Ploplis VA, Castellino FJ, 2016a Phenotypic differentiation of Streptococcus pyogenes populations is induced by recombination-driven gene-specific sweeps. Sci. Rep 6, 36644. [PubMed: 27821851]

Bao YJ, Liang Z, Mayfield JA, Donahue DL, Carothers KE, Lee SW, Ploplis VA, Castellino FJ, 2016b Genomic characterization of a Pattern D Streptococcus pyogenes emm53 isolate reveals a genetic rationale for invasive skin tropicity. J. Bacteriol 198, 1712–1724. [PubMed: 27044623]

Berge A, Sjobring U, 1993 PAM, a novel plasminogen-binding protein from Streptococcus pyogenes. J. Biol. Chem 268, 25417–25424. [PubMed: 8244975]

Bessen DE, 2016. Molecular basis of serotyping and the underlying genetic organization of Streptococcus pyogenes in Streptococcus pyogenes: Basic Biology to Clinical Manifestations, Ferretti JJ, Stevens DL, Fischetti VA, editors. 2, 2016.

Bhattacharya S, Liang Z, Quek AJ, Ploplis VA, Law R, Castellino FJ, 2014 Dimerization is not a determining factor for functional high affinity human plasminogen binding by the group A streptococcal virulence factor PAM and is mediated by specific residues within the PAM a1a2 domain. J. Biol. Chem 289, 21684–21693. [PubMed: 24962580]

Buffalo C, Bahn-Suh AJ, Hirakis SP, Biswas T, Amaro RE, Nizet V, Ghosh P, 2016 Conserved patterns hidden within group A streptococcus M protein hypervariability recognize human C4b-binding protein. Nat. Microbiol 1, 16155. [PubMed: 27595425]

Castellino FJ, Ploplis VA, 2003 Human plasminogen: structure, activation, and function. Plasminogen Structure, activation, and regulation Kluwer Academic/Plenum Publishers, 3–17.

Castellino FJ, Ploplis VA, Powell JR, Strickland DK, 1981 The existence of independent domain structures in human lys77-plasminogen. J. Biol. Chem 256, 4778–4782. [PubMed: 7228856]

Chandrahas V, Glinton K, Liang Z, Donahue DL, Ploplis VA, Castellino FJ, 2015 Direct host plasminogen binding to bacterial surface M-protein in Pattern D strains of Streptococcus pyogenes Is required for activation by Its natural coinherited SK2b protein. J. Biol. Chem 290, 18833–18842. [PubMed: 26070561]

Chen J, Im W, Brooks CL, 2004 Refinement of NMR structures using implicit solvent and advanced sampling techniques. J. Am. Chem. Soc 126, 16038–16047. [PubMed: 15584737]

Chen VB, Arendall WB, Headd JJ, Keedy DA, Immormino RM, Kapral GJ, Murray LW, Richardson JS, Richardson DC, 2010 MolProbity: all-atom structure validation for macromolecular crystallography. Acta Crystallogr. D Biol. Crystallogr 66, 12–21. [PubMed: 20057044]

Clubb RT, Thanabal V, Wagner G, 1992 A new 3D HN(CA)HA experiment for obtaining fingerprint HN-Halpha peaks in 15N- and 13C-labeled proteins. J. Biomol. NMR 2, 203–210. [PubMed: 1422153]

Courtney HS, Hasty DL, Dale JB, 2006 Anti-phagocytic mechanisms of Streptococcus pyogenes: binding of fibrinogen to M-related protein. Mol .Microbiol 59, 936–947. [PubMed: 16420362]

Gasteiger E, Gattiker A, Hoogland C, Ivanyi I, Appel RD, Bairoch A, 2003 ExPASy: The proteomics server for in-depth protein knowledge and analysis. Nucl. Acids Res 31, 3784–3748. [PubMed: 12824418]

Ghosh P, 2011 The nonideal coiled coil of M protein and its multifarious functions in pathogenesis. Adv. Exp. Med. Biol 715, 197–211. [PubMed: 21557065]

Glinton K, Beck J, Liang Z, Qiu C, Lee SW, Ploplis VA, Castellino FJ, 2017 Variable region in streptococcal M-proteins provides stable binding with host fibrinogen for plasminogen-mediated bacterial invasion. J. Biol. Chem 292, 6775–6785. [PubMed: 28280245]

Grzesiek S, Bax A, 1992 Correlatting backbone amide and side-chain resonances in larger proteins by multiple relayed thriple resonance NMR. J. Am. Chem. Soc 114, 6291–6293.

Grzesiek S, Anglister J, Bax A, 1993a Correlation of backbone amide and aliphatic side-chain resonances in C-13/N-15-enriched proteins by isotropic mixing of C-13 magnetization. J. Magn. Reson 101, 114–119.

Grzesiek S, Anglister J, Ren H, Bax A, 1993b 13C line narrowing by 2H decoupling in 2H/13C/15N-enriched proteins. Application to triple resonance 4D J connectivity of sequential amides. J. Am. Chem. Soc 115, 4369–4370.

Gustafsson MC, Lannergård J, Nilsson OR, Kristensen BM, Olsen JE, Harris CL, Ufret-Vincenty RL, Stålhammar-Carlemalm M, Lindahl G, 2013 Factor H binds to the hypervariable region of many Streptococcus pyogenes M proteins but does not promote phagocytosis resistance or acute virulence. PLoS Pathog. 9, e1003323. [PubMed: 23637608]

Ikura M, Kay LE, Tschudin R, Bax A, 1990 3-Dimensional NOESY-HMQC spectroscopy of a C-13-labeled protein. J. Magn. Reson 86, 204–209.

Kay L, Keifer P, Saarinen T, 1992 Pure absorption gradient enhanced heteronuclear single quantum correlation spectroscopy with improved sensitivity. J. Am. Chem. Soc 114, 10663–10665.

Kay LE, Ikura M, Tschudin R, Bax A, 1990 Three-dimensional triple-resonance NMR spectroscopy of isotopically enriched proteins. J. Magn. Reson 89, 496–514.

Lahteenmaki K, Kuusela P, Korhonen TK, 2000 Plasminogen activation in degradation and penetration of extracellular matrices and basement membranes by invasive bacteria. Methods 21, 125–132. [PubMed: 10816373]

Laskowski RA, MacArthur MW, Moss DS, Thornton JM, 1993 PROCHEK: a program to check the stereochemical quality of protein structures. J. Appl. Cryst 26, 283–291.

Laue TM, Shah BD, Pelletier SL, 1992 Computer-aided interpretation of analytical sedimentation data for proteins, p. 90–125, in: Harding SE, et al., Eds.), Analytical Ultracentrifugation in Biochemistry and Polymer Science, Royal Society of Chemistry, Cambridge, UK.

Lee W, Westler WM, Bahrami A, Eghbalnia HR, Markley JL, 2009 PINE-SPARKY: graphical interface for evaluating automated probabilistic peak assignments in protein NMR spectroscopy. Bioinformatics 25, 2085–2087. [PubMed: 19497931]

Liang Z, Zhang Y, Agrahari G, Chandrahas V, Glinton K, Donahue DL, Balsara RD, Ploplis VA, Castellino FJ, 2013 A natural inactivating mutation in the CovS component of the CovRS regulatory operon in a pattern D Streptococcal pyogenes strain influences virulence-associated genes. J. Biol. Chem 288, 6561–6573. [PubMed: 23316057]

Markley JL, Bax A, Arata Y, Hilbers CW, Kaptein R, Sykes BD, Wright PE, Wüthrich K, 1998 Recommendations for the presentation of NMR structures of proteins and nucleic acids. IUPAC-IUBMB-IUPAB Inter-Union Task Group on the Standardization of Data Bases of Protein and Nucleic Acid Structures Determined by NMR Spectroscopy. J. Biomol. NMR 12, 1–23. [PubMed: 9729785]

McNamara C, Zinkernagel AS, Macheboeuf P, Cunningham MW, Nizet V, Ghosh P, 2008 Coiled-coil irregularities and instabilities in group A Streptococcus M1 are required for virulence. Science 319, 1405–1408. [PubMed: 18323455]

Miles LA, Dahlberg CM, Plescia J, Felez J, Kato K, Plow EF, 1991 Role of cell-surface lysines in plasminogen binding to cells: Identification of a-enolase as a candidate plasminogen receptor. Biochemistry 30, 1682–1691. [PubMed: 1847072]

Mori S, Abeygunawardana C, Johnson MO, van Zijl PC, 1995 Improved sensitivity of HSQC spectra of exchanging protons at short interscan delays using a new fast HSQC (FHSQC) detection scheme that avoids water saturation. J. Magn. Reson. B 108, 94–98. [PubMed: 7627436]

Nilsen SL, DeFord ME, Prorok M, Chibber BAK, Bretthauer RK, Castellino FJ, 1997 High-level secretion in Pichia pastoris and biochemical characterization of the recombinant kringle 2 domain of tissue-type plasminogen activator. Biotech. Appl. Biochem 25, 63–74.

Nitanai Y, Minakata S, Maeda K, Oda N, Maéda Y, 2007 Crystal structures of tropomyosin: flexible coiled-coil. Adv. Exp. Med. Biol 592, 135–151.

Ottiger M, Delaglio F, Bax A, 1998 Measurement of J and dipolar couplings from simplified two-dimensional NMR spectra. J. Magn. Reson 131, 373–378. [PubMed: 9571116]

Pancholi V, Fischetti VA, 1998 alpha-enolase, a novel strong plasmin(ogen) binding protein on the surface of pathogenic streptococci. J. Biol. Chem 273, 14503–14515. [PubMed: 9603964]

Qiu C, Yuan Y, Liang Z, Lee SW, Ploplis VA, Castellino FJ, 2019 Variations in the secondary structures of PAM proteins influence their binding affinities to human plasminogen. J. Struct. Biol 206, 193–203. [PubMed: 30880082]

Qiu C, Yuan Y, Zajicek J, Liang Z, Balsara RD, Brito-Robionson T, Lee SW, Ploplis VA, Castellino FJ, 2018 Contributions of different modules of the plasminogen-binding Streptococcus pyogenes M-protein that mediate its functional dimerization. J. Struct. Biol 204, 151–164. [PubMed: 30071314]

Ringdahl U, Svensson M, Wistedt AC, Renn T, Kellner R, Muller-Esterl W, Sjobring U, 1998 Molecular co-operation between protein PAM and streptokinase for plasmin acquisition by Streptococcus pyogenes. J. Biol. Chem 272, 6424–6230.

Rios-Steiner JL, Schenone M, Mochalkin I, Tulinsky A, Castellino FJ, 2001 Structure and binding determinants of the recombinant kringle-2 domain of human plasminogen to an internal peptide from a group A Streptococcal surface protein. J. Mol. Biol 308, 705–719. [PubMed: 11350170]

Sanderson-Smith ML, Dowton M, Ranson M, Walker MJ, 2007 The plasminogen-binding group A streptococcal M protein-related protein Prp binds plasminogen via arginine and histidine residues. J. Bacteriol 189, 1435–1440. [PubMed: 17012384]

Sanderson-Smith ML, Dinkla K, Cole JN, Cork AJ, Maamary PG, McArthur JD, Chhatwal GS, Walker MJ, 2008 M protein-mediated plasminogen binding is essential for the virulence of an invasive Streptococcus pyogenes isolate. FASEB J. 22, 2715–2722. [PubMed: 18467595]

Schenone MM, Warder SE, Martin JA, Prorok M, Castellino FJ, 2000 An internal histidine residue from the bacterial surface protein, PAM, mediates its binding to the kringle-2 domain of human plasminogen. J. Pept. Res 56, 438–445. [PubMed: 11152303]

Shen Y, Lange O, Delaglio F, Rossi P, Aramini JM, Liu G, Eletsky A, Wu Y, Singarapu KK, Lemak A, Ignatchenko A, Arrowsmith CH, Szyperski T, Montelione GT, Baker DM, Bax A, 2008 Consistent blind protein structure generation from NMR chemical shift data. Proc. Natl. Acad. Sci. USA 105, 4685–4690. [PubMed: 18326625]

Stewart CM, Buffalo CZ, Valderrama JA, Henningham A, Cole JN, Nizet V, Ghosh P, 2016 Coiled-coil destabilizing residues in the group A Streptococcus M1 protein are required for functional interaction. Proc. Natl. Acad. Sci. USA 113, 9515–9520. [PubMed: 27512043]

Sumitomo T, Nakata M, Higashino M, Terao Y, Kawabata S, 2013 Group A streptococcal cysteine protease cleaves epithelial junctions and contributes to bacterial translocation. J. Biol. Chem 288, 13317–13324. [PubMed: 23532847]

Sumitomo T, Nakata M, Higashino M, Yamaguchi M, Kawabata S, 2016 Group A Streptococcus exploits human plasminogen for bacterial translocation across epithelial barrier via tricellular tight junctions. Sci. Rep 7, 20069. [PubMed: 26822058]

Sun H, Ringdahl U, Homeister JW, Fay WP, Engelberg NC, Yang AY, Rozek LS, Wang X, Sjobring U, Ginsburg D, 2004 Plasminogen is a critical host pathogenicity factor for Group A streptococcal infection. Science 305, 1283–1286. [PubMed: 15333838]

Talluri S, Wagner G, 1996 An optimized 3D NOESY-HSQC. J. Magn. Reson. Ser. B 112, 200–205. [PubMed: 8812906]

van Zundert GCP, Rodrigues JPGLM, Trellet M, Schmitz C, Kastritis PL, Karaca E, Melquiond ASJ, van Dijk M, de Vries SJ, Bonvin AMJJ, 2016 The HADDOCK2.2 web server: User-friendly integrative modeling of biomolecularcomplexes. J. Mol. Biol 428, 720–725. [PubMed: 26410586]

Wang M, Prorok M, Castellino FJ, 2010a NMR backbone dynamics of VEK-30 bound to the human plasminogen kringle 2 domain. Biophys. J 99, 302–312. [PubMed: 20655859]

Wang M, Zajicek J, Geiger JH, Prorok M, Castellino FJ, 2010b Solution structure of the complex of VEK-30 and plasminogen kringle 2. J. Struct. Biol 169, 349–359. [PubMed: 19800007]

Wen J, Arakawa T, Wypych J, Langley KE, Schwartz MG, Philo JS, 1997 Chromatographic determination of extinction coefficients of non-glycosylated proteins using refractive index (RI) and UV absorbance (UV) detectors: Applications for studying protein interactions by size exclusion chromatography with light-scattering, UV, and RI detectors. Tech. Prot. Chem 8, 113–119.

Whitnack E, Beachey EH, 1982 Antiopsonic activity of fibrinogen bound to M protein on the surface of group A streptococci. J Clin Invest. 69, 1042–1045. [PubMed: 7042754]

Williamson MP, 2013 Using chemical shift perturbation to characterise ligand binding. Prog. Nucl. Magn. Reson. Spectrosc 73, 1–16. [PubMed: 23962882]

Wistedt AC, Ringdahl U, Müller-Esterl W, Sjøbring U, 1995 Identification of a plasminogen-binding motif in PAM, a bacterial surface protein. Mol. Microbiol 18, 569–578. [PubMed: 8748039]

Wistedt AC, Kotarsky H, Marti D, Ringdahl U, Castellino FJ, Schaller J, Sjobring U, 1998 Kringle 2 mediates high affinity binding of plasminogen to an internal sequence in streptococcal surface protein PAM. J. Biol. Chem 273, 24420–24424. [PubMed: 9733732]

Wittekind M, Mueller L, 1993 HNCACB, A high-sensitivity 3D NMR experiment to correlate amide-proton and nitrogen resonances with the alpha-carbon and beta-carbon resonances in proteins. J. Magn. Reson 101, 201–205.

Yuan Y, Zajicek J, Qiu C, Chandrahas V, Lee SW, Ploplis VA, Castellino FJ, 2017 Conformationally organized lysine isosteres in *Streptococcus pyogenes* M protein mediate direct high-affinity binding to human plasminogen. J. Biol. Chem 292, 15016–15027. [PubMed: 28724633]

Highlights

- Solution structural determination by high-resolution NMR of the A-domain of PAM reveals occupancy by two molecules of $K2_{hPg}$ on opposite faces of the A-domain helix.
- $K2_{hPg}$ binds to PAM through repeating sequences (*a1a2*-repeats) in the A domain of PAM and uses the same lysine binding site for its interaction with each of the two *a*-repeats.
- $K2_{hPg}$ binds more tightly to the *a2*-region than the *a1*-region due to different sets of exosite interactions.

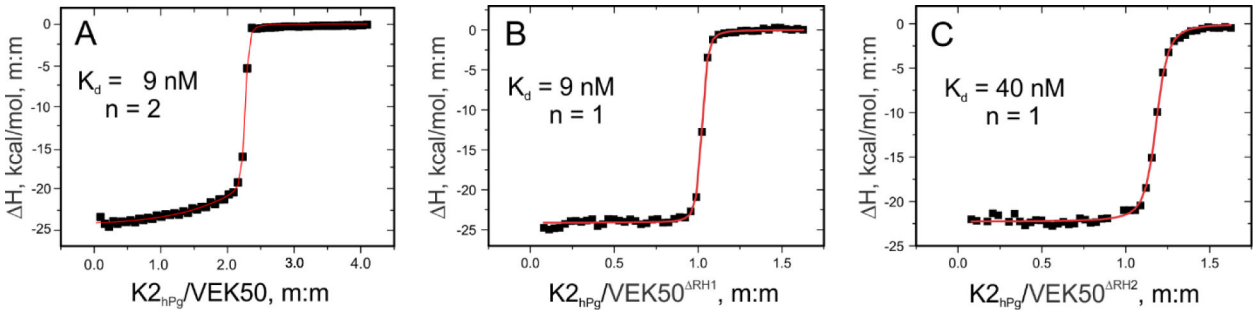

Fig. 1. Isothermal titration calorimetric (ITC) analysis of the binding of VEK50 peptides to $K2_{hPg}$.

Binding isotherms at 25° C for the titration of $K2_{hPg}$ (900 μM stock) into: (A) 40 μM VEK50 in the cell, (B) 40 μM VEK50$^{\Delta RH1}$ in the cell, and (C) 40 μM VEK50$^{\Delta RH2}$ in the cell. The heats liberated upon binding were measured as a function of the concentration of $K2_{hPg}$. The red lines in Panels A-C represent the best-fits of the experimental data (black symbols) to a two-site model (A) and one-site models (B, C).

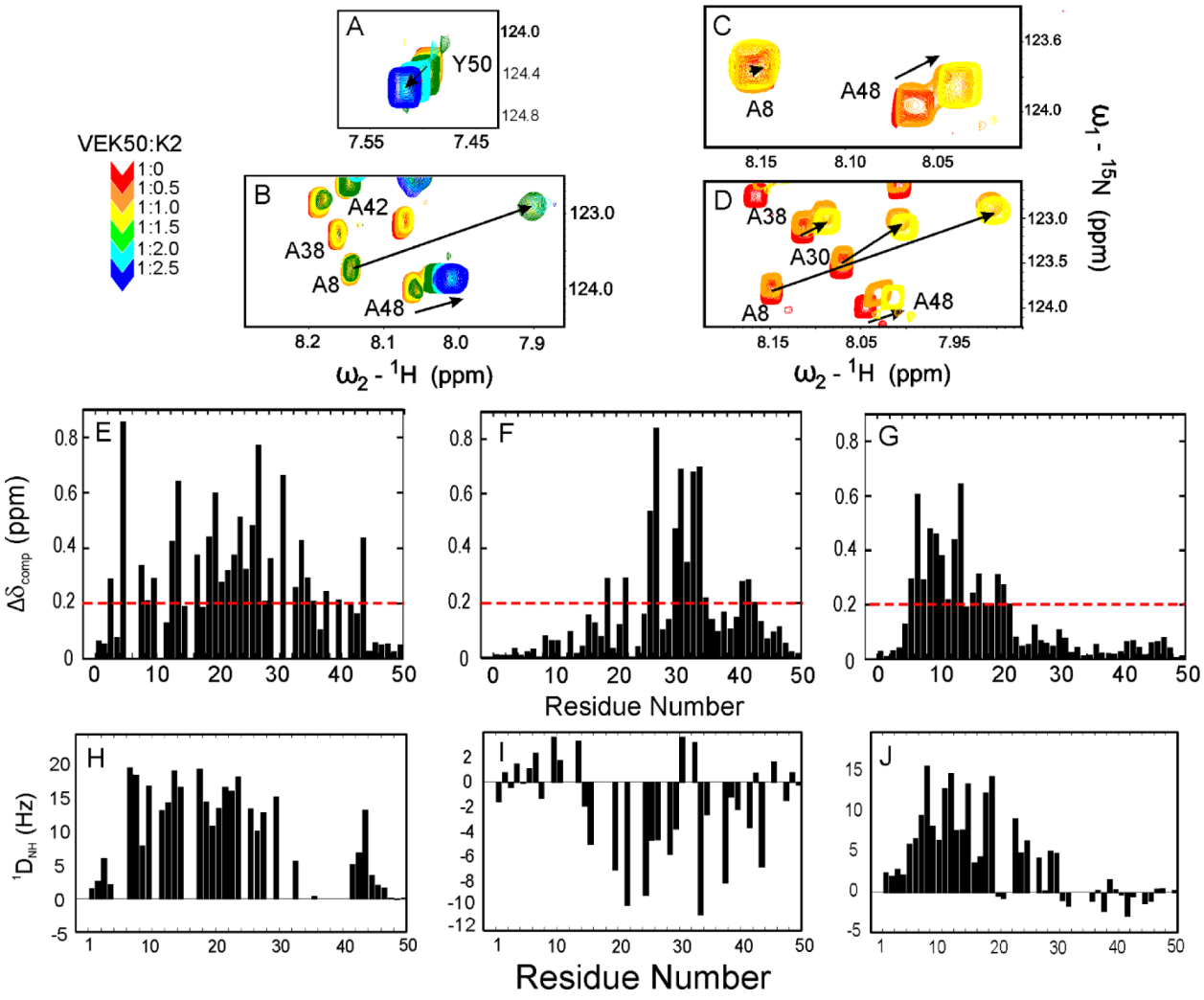

Fig. 2. NMR spectroscopic analysis of the interactions between VEK50 peptides and $K2_{hPg}$.

The stoichiometry between VEK50 and $K2_{hPg}$ was confirmed from chemical shift changes of some residues in overlaid ^{15}N-HSQC spectra of: (A, B) ^{15}N-VEK50; (C) ^{15}N-VEK50$^{\Delta RH1}$; and (D) ^{15}N-VEK50$^{\Delta RH2}$ by titrating ^{15}N-labeled VEK50 peptides with unlabeled $K2_{hPg}$ at molar ratios of (VEK50 peptide:$K2_{hPg}$) of 1:0.5 (orange), 1:1 (yellow), 1.1.5 (green), 1:2 (cyan), and 1:2.5 (blue). The sample buffer was 20 mM Bis-Tris-d19, pH 6.8 at 25° C. (D-F) Chemical-shift differences ($^{\Delta}\delta$ ppm) between apo- and bound-forms of VEK50 peptides. The $^{\Delta}\delta$ ppm values of: (E) WT-VEK50, (F) VEK50$^{\Delta RH1}$, and (G) VEK50$^{\Delta RH2}$ are plotted against the residue numbers. (H–J) Plots of $^{1}D_{NH}$ RDCs as a function of the residue number for ^{15}N-VEK50 (H), ^{15}N-VEK50$^{\Delta RH1}$ (I), and ^{15}N-VEK50$^{\Delta RH2}$ (J), each in complex with $K2_{hPg}$ at molar ratios of 1:2, 1:1, and 1:1. The measurements were performed on samples in filamentous phages Pf1 (10 mg/ml) using two-dimensional IPAP[^{15}N/^{1}H]HSQC experiments (Ottiger et al., 1998). Residues with severe peak overlap or poor signal-to-noise ratios were excluded.

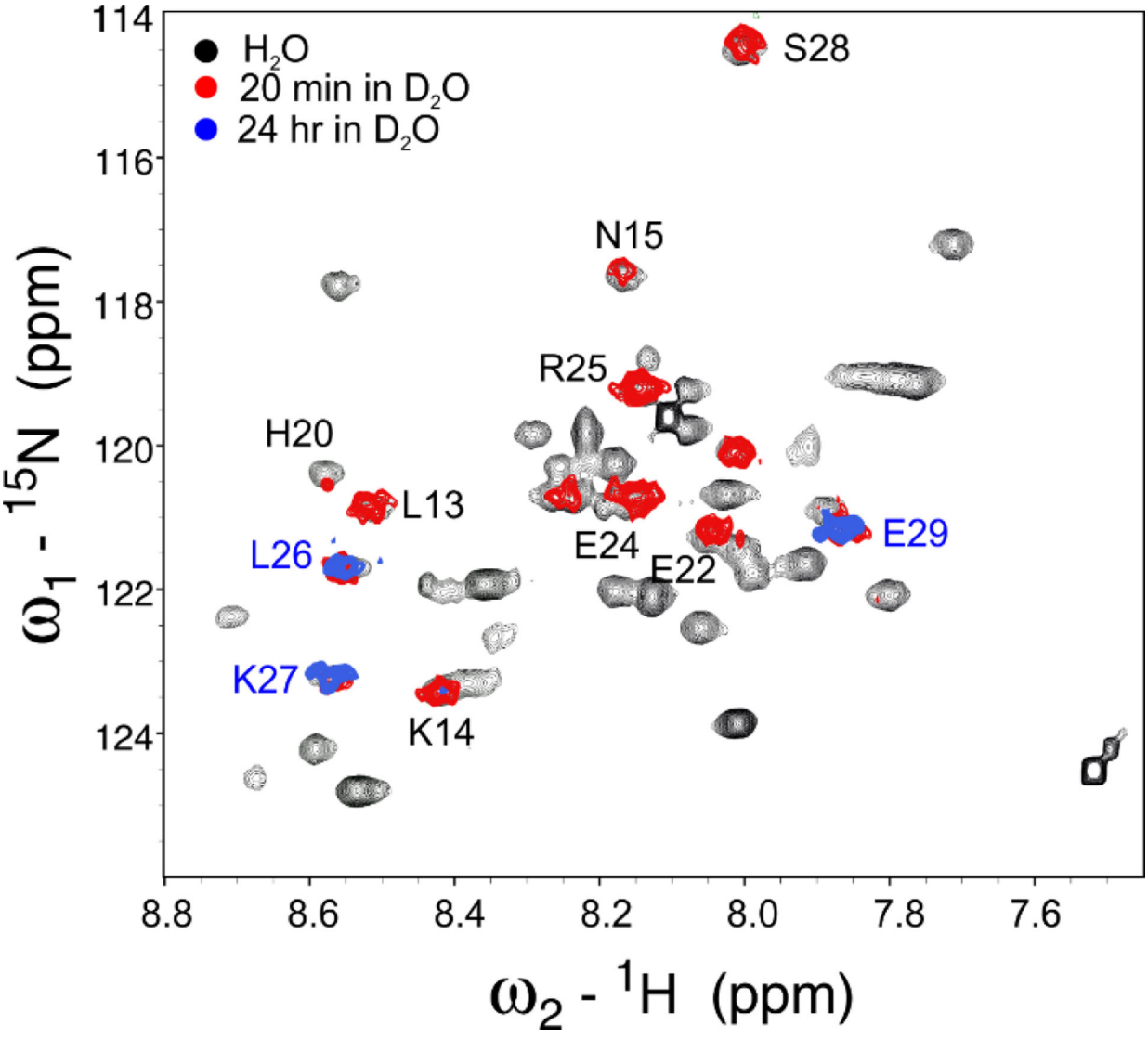

Fig. 3. $^{1}H/^{2}H$ exchange of VEK50.

Overlays of the ^{1}H-^{15}N HSQC spectra of the complex of ^{15}N-VEK50/unlabeled $K2_{hPg}$ obtained in BisTris-d19, pH 6.8 (black), at 20 min (red) and 24 hr (blue) after the lyophilized complex powder was re-dissolved in $^{2}H_2O$ at 25° C. The assignments of the backbone amide signals are indicated by the respective single-letter codes and residue numbers.

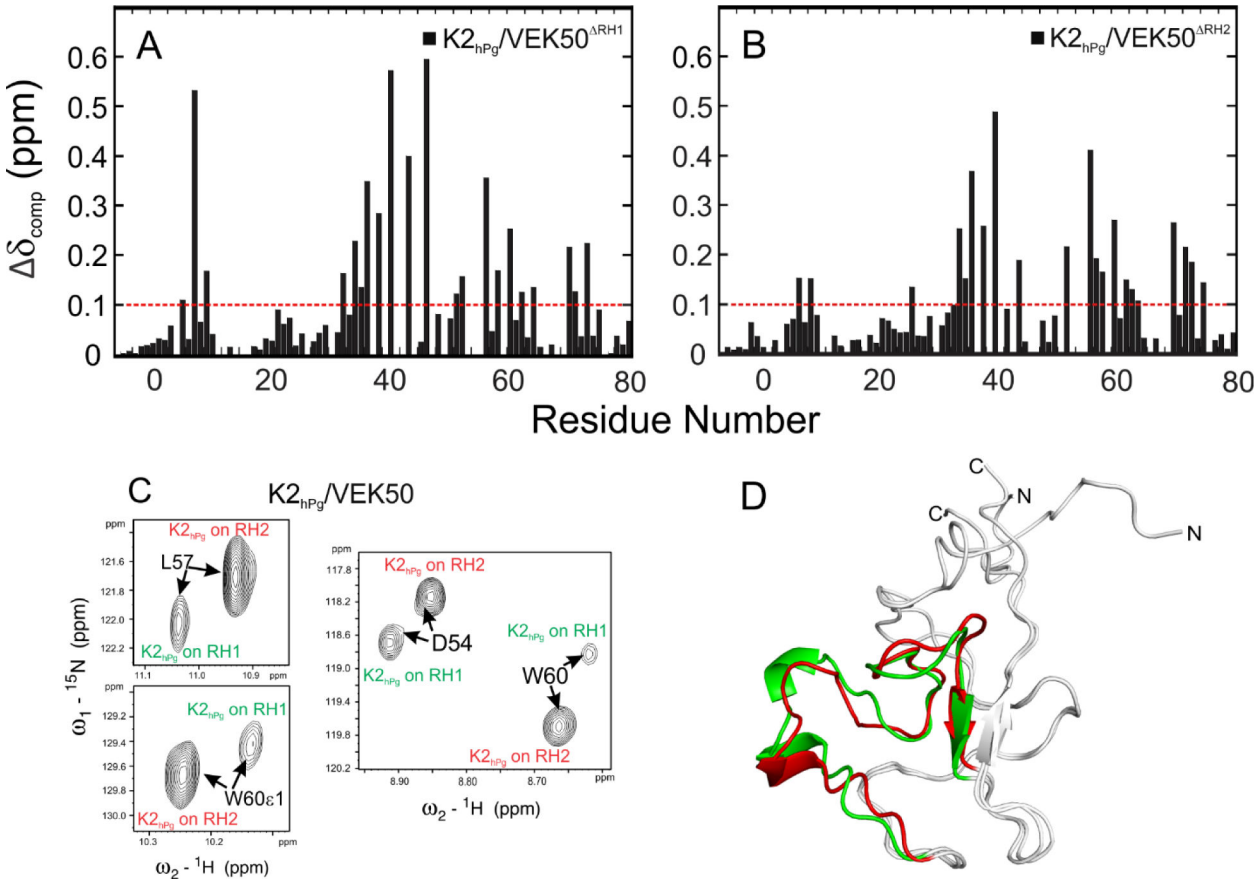

Fig. 4. Differences in the binding sites of $K2_{hPg}$ upon its interaction with $VEK50^{\Delta RH1}$ and $VEK50^{\Delta RH2}$.

Combined chemical shift changes ($^{\Delta}\delta$ ppm) along the sequence of $K2_{hPg}$ between apo-$K2_{hPg}$ and $K2_{hPg}$ bound to: (A) $VEK50^{\Delta RH1}$ and (B) $VEK50^{\Delta RH2}$. (C) Residues in the VEK50-bound $K2_{hPg}$ exhibit two resonance signals as shown in the expanded ^{15}N-HSQC spectra. (D) The refined solution structural backbones of $K2_{hPg}$ bound to $VEK50^{\Delta RH1}$ (red) and $VEK50^{\Delta RH2}$ (green) are overlaid and shown in as ribbons.

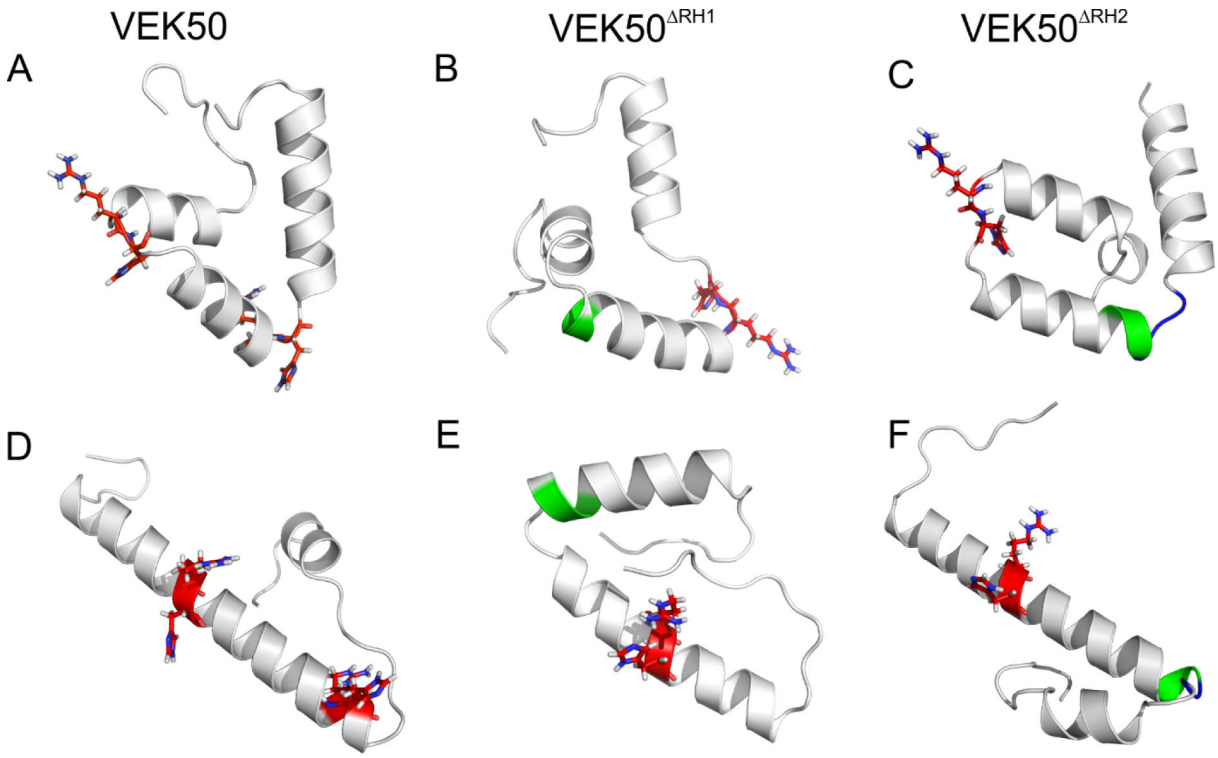

Fig. 5. Comparison of the solution structures of apo- and $K2_{hPg}$-bound VEK peptides.

(A, D) VEK50; (B, E) $VEK50^{\Delta RH1}$; and (C, F) VEK50 $^{\Delta RH2}$. A, B, and C represent the apo-forms of the indicated peptides; D, E, and F represent the peptides bound to $K2_{hPg}$. The RH1 and RH2 backbones are shown as red sticks and Ala-Ala backbones are colored green in the ribbons.

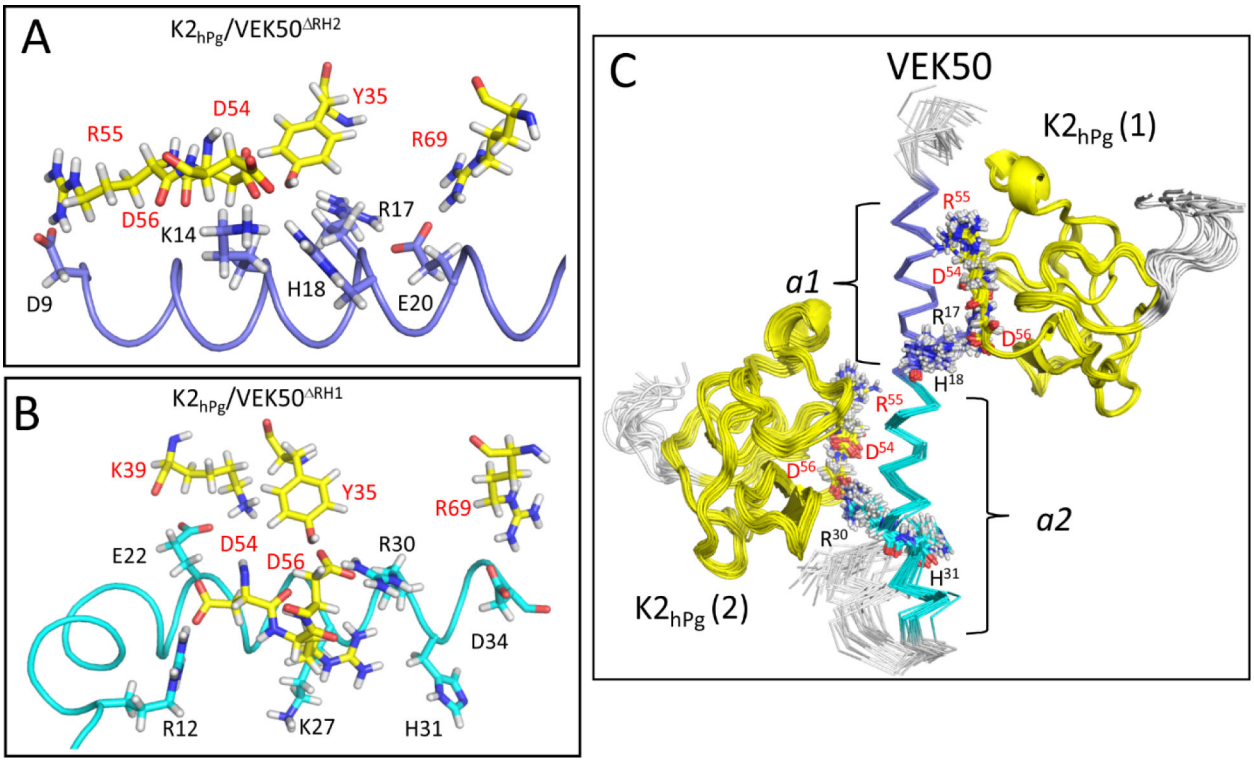

Fig. 6. Solution binding models of the $K2_{hPg}$/VEK50 peptides derived from Xplor-NIH and HADDOCK.

The lowest-energy conformation was used for the representation of: (A) $K2_{hPg}$ /$VEK50^{\Delta RH2}$ and (B) $K2_{hPg}$/$VEK50^{\Delta RH1}$. (C) Superposition of backbone traces of the 20 lowest-energy NMR structures of $K2_{hPg}$ /VEK50 is shown. $VEK50^{\Delta RH1}$ and $VEK50^{\Delta RH2}$ bind to $K2_{hPg}$ at a molar ratio of 1:1, whereas VEK50 binds to $K2_{hPg}$ at a molar ratio of 1:2. Residues having H-bond interactions with $K2_{hPg}$ and having close contact (~3 Å) are labeled and shown as sticks. $K2_{hPg}$ is colored yellow whereas the *a1*- and *a2*-repeats of VEK50 are colored magenta and cyan, respectively.

Table 1.

Amino acid sequences of truncated peptides from PAM_{AP53} and hPg

Peptides	Amino Acid Sequences[a]
VEK50	GS(V[1]EKLTADAELQRLKNE**R[17]H[18]**EEAELERLKSE**R[30]H[31]**DHDKKEAERKALEDKLAD)Y
VEK50$^{\Delta RH1}$	GS(V[1]EKLTADAELQRLKNE**A[17]A[18]**EEAELERLKSE**R[30]H[31]**DHDKKEAERKALEDKLAD)Y
VEK50$^{\Delta RH2}$	GS(V[1]EKLTADAELQRLKNE**R[17]H[18]**EEAELERLKSE**A[30]A[31]**DHDKKEAERKALEDKLAD)Y
$K2_{hPg}$	Y-[7]VEFSEE(C[1]MHC[4]SGENYDGKISKTMSGLECQAWDSQSPHAHGYIPSKFPNKNLKKNYCRNPDRE[56]LRPWCFTTDPNKRWEY[72] CDIPRC[78])AA

[a]Residues outside the parentheses in all cases are exogenous to PAM or $K2_{hPg}$.

Table 2.

Molecular masses of truncated peptides from PAM_{AP53} and the complexes with $K2_{hPg}$

Peptide	Theoretical (Da)	MALDI-TOF (Da)[a]	AUC (Da)[b]	
			Apo-peptides	Peptide + $K2_{hPg}$
VEK50	6,159	6,166	6,300 ± 800	27,300 ± 850
$VEK50^{\Delta RH1}$	6,008	6008	5,600 ± 500	16,150 ± 1,000
$VEK50^{\Delta RH2}$	6,008	6010	5,700 ± 600	16,400 ± 1,000
$K2_{hpg}$	10,151	10,155	10,260 ± 800	above

[a] Molecular masses of the protein linear sequence from MALDI-TOF.

[b] Weight-average molecular mass of proteins in solution from AUC experiments at 25° C.